



An imino nitroxide free radical: experimental and theoretical spin density and electronic structure

A. Zheludev^{a,*}, M. Bonnet^a, B. Delley^b, A. Grand^c, D. Luneau^c, L. Örstöm^c,
E. Ressouche^a, P. Rey^c, J. Schweizer^a

^a CEA, CENG / DRFMC / SPSMS / MDN, 17 rue des Martyrs, 38054 Grenoble Cedex 9, France

^b Paul Scherer Institut Zürich, Badenerstr. 569, 8048 Zürich, Switzerland

^c CEA, CENG / DRFMC / SESAM, 17 rue des Martyrs, 38054 Grenoble Cedex 9, France

Received 8 June 1994; in revised form 12 September 1994

Abstract

An imino nitroxide, the 2-(3-nitrophenyl)-4,4,5,5-tetramethyl-4,5-dihydro-1H-imidazol-1-oxyl (m-NPIM), a potential building block for molecular-based magnets, was investigated by conventional and polarized neutron single crystal diffraction. Several methods, including the recently developed Default Model Maximum of Entropy (DMME) technique, were used to reconstruct the spin density distribution in the radical. Quantitative (atomic spin populations) and qualitative (shape of the spin density around the nuclei) results were obtained. Our data provide the basis for the discussion of the electronic configuration of imino nitroxides. The nodes of the singly occupied molecular orbital (SOMO) were directly observed. The spin polarization effect, which gives rise to negative spin densities of several atomic sites in the radical and is liable for the spin density transfer to the nitrophenyl group, is discussed. The spin distribution is compared to that previously observed experimentally in nitronyl nitroxides and with theoretical predictions obtained by density functional first principle calculations.

1. Introduction

Conjugated nitroxides such as nitronyl nitroxides are among the most versatile spin carriers involved in the design of magnetic molecular materials [1]. Their delocalized electronic structure is responsible for peculiar spin density distributions which provide pathways for intermolecular magnetic interactions and optimum spin correlation when they are used as bridging ligands towards metal ions [2]. As a result,

the only representatives of non-ionic organic ferromagnets are nitroxide free radicals [3,4]. Understanding of the magnetic properties of these species relies mainly on recently reported experimental polarized neutron diffraction studies [5,6].

Although imino nitroxides (Fig. 1a) are closely related to nitronyl nitroxides, much less work has been devoted to the studies of these materials. Indeed, synthetic difficulties [7] have been a strong limitation to the efforts aimed at developing exchange coupled species based on imino nitroxides. We have recently overcome these difficulties and reported our studies of the free radicals themselves [8] and their coordination compounds [9,10]. Compared to the nitronyl nitroxides, peculiar coordination

* Corresponding author. Current address: Brookhaven National Laboratory, Upton, NY 11973-5000, USA. Fax: +1-516-282-2918; email: zhelud@solids.phys.bnl.gov.

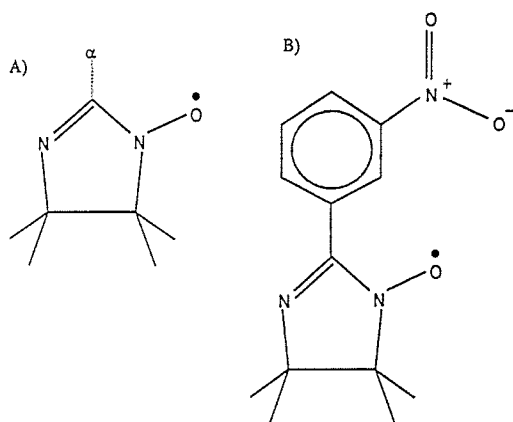


Fig. 1. (a) General formula of imino nitroxides. (b) Structural formula of the 2-(3-nitrophenyl)-4,4,5,5-tetramethyl-4,5-dihydro-1H-imidazol-1-oxyl (m-NPIM).

chemistry based on the imino nitrogen atom was observed and exceptional magnetic behavior such as ferromagnetic-metal-nitroxide interactions persisting at room temperature were characterized [9].

With the aim to give a quantitative support to these findings we decided to undertake an experimental determination of the spin density in this family of nitroxides. The choice of a compound turned out to be very difficult. Several crystal structures of these radicals were investigated which showed disorder, the nitroxyl oxygen atom being modeled with half occupancy on both nitrogens [11]. Further difficulties came from antiferromagnetic behaviors at low temperature [11]. Finally, we succeeded to grow a large crystal of 2-(3-nitrophenyl)-4,4,5,5-tetramethyl-4,5-dihydro-1H-imidazol-1-oxyl, m-NPIM (Fig. 1b), whose structure is not disordered and in which intermolecular interactions are weak. The results of the polarized neutron diffraction study which we report herein, are compared to those obtained previously for a nitronyl nitroxide [5] (2-phenyl-4,4,5,5-tetramethyl-4,5-dihydro-1H-imidazol-3-oxide-1-oxyl, PNN) and to theoretical first principle calculations.

2. The experimental technique

Polarized neutron diffraction is a very useful technique for spin density studies in molecular crystals. The measurements are usually performed in the paramagnetic state. A periodic aligned magnetization

(spin) density $S(r) = S(r)\hat{z}$ is induced in a single-crystal sample by applying a strong magnetic field (\hat{z} being the field direction) at sufficiently low temperature. Using a polarized neutron beam one measures the so-called flipping ratios R of Bragg reflections (hkl) [12], which are related to the magnetic structure factors $F_M(hkl)$, the spatial Fourier components of $S(r)$. In the case of a centrosymmetric structure, the F_M 's may be directly deduced from the experimental flipping ratios if the exact crystal structure of the compound is known (see for instance Ref. [12]). The experiment has to include two steps. In the first step the crystal structure is refined at low temperature using conventional neutron diffraction. In the second step the flipping ratios are collected (polarized neutron diffraction).

3. Experimental section

3.1. Sample characterization

Translucent red regularly shaped crystals of m-NPIM, sufficiently large to be used for neutron diffraction were prepared by slow evaporation at room temperature of a saturated hexane solution. The room temperature crystal structure of our samples was determined by X-ray diffraction. m-NPIM crystallizes in the centrosymmetric monoclinic $P2_1/c$ (no. 14) space group, the room-temperature cell constants being $a = 13.180 \text{ \AA}$, $b = 7.379 \text{ \AA}$, $c = 27.511 \text{ \AA}$ and $\beta = 91.02^\circ$ respectively [13].

Magnetization and dc susceptibility measurements were performed on a commercial Quantum Design ac SQUID magnetometer. A susceptibility curve was measured at $H = 5 \text{ kOe}$ in the temperature range 2–300 K. The dependence indicates weak antiferromagnetic interaction and is well fit by a $\chi = C/(T + \theta)$ law with $\theta = 1.2 \text{ K}$.

To obtain the (000) magnetic structure factor, an $M(T)$ curve in a field of 4.65 T (polarized neutron experimental conditions) was also measured. For a temperature $T = 1.6 \text{ K}$ at which the flipping ratios were collected spin $\frac{1}{2}$ saturation was found to be 85.6%.

3.2. Low-temperature structure determination

To calculate the F_M 's and to extract the magnetic information from the flipping ratios, detailed knowl-

edge of the low-temperature crystal structure is required. It was determined in a conventional neutron diffraction experiment on the DN4 4-circle diffractometer at the reactor SILOE (CEN Grenoble, France). A single crystal in the form of a regular slab of $(5.3 \times 1.8 \times 1.0) \text{ mm}^3$ was preliminary oriented by Laue X-ray diffraction. The larger rectangular face was identified as (100) and its edges as [010] and [001]. Once mounted on the neutron diffractometer, the crystal was cooled down to the experimental temperature of 30 K by means of a 3-stage Joule–Thompson refrigerator. The space group remains unchanged at low temperature. After computer centering of 22 Bragg peaks the cell constants were determined to be $a = 13.15(3) \text{ \AA}$, $b = 7.29(2) \text{ \AA}$, $c = 26.98(4) \text{ \AA}$ and $\beta = 91.45(11)^\circ$. ω -scans were used to measure 2180 independent Bragg intensities with $\sin \theta/\lambda$ up to 0.42 \AA^{-1} ($\lambda = 1.189 \text{ \AA}$). Integration of peak intensities was done during experimental runtime using the COLL5 program [14].

3.3. Polarized neutron diffraction

The experiment was performed on the DN2 polarized neutron lifting counter diffractometer at the SILOE reactor. A beam of wavelength $\lambda = 1.205 \text{ \AA}$ and polarization of -94% (Heussler alloy monochromator) was used. The $\lambda/2$ beam contamination was 0.27% . Two series of measurements were carried out. In the first series a $(5.7 \times 5.3 \times 1.1) \text{ mm}^3$ regularly shaped crystal was mounted with the b axis collinear to the 4.65 T field of a split-coil cryomagnet. In this geometry the $(h 0 l)$, $(h 1 l)$ and $(h 2 l)$ reciprocal space planes were accessible for measurements. The flipping ratios were measured at $T = 1.6 \text{ K}$. In the second series the same crystal was rotated to align the c axis parallel to the field. Flipping ratios in the planes $(h k 0)$, $(h k 1)$, $(h k 2)$ and $(h k 4)$ were collected at $T = 1.6 \text{ K}$. In both series the measurements were performed for $\sin \theta/\lambda$ up to 0.38 \AA^{-1} . Altogether 248 independent flipping ratios were measured.

4. Data treatment and results

4.1. Structural studies

The structure was refined using the least-squares program ORXFLS [15]. Absorption corrections were

made by calculating the mean crystal traversing path for each reflection. All atoms were treated with isotropic thermal parameters. Extinction was found to be very small and was not taken into account.

Using 2180 data and 286 variables the value of $\chi^2 = 1.56$ (weighted R -factor = 9.3%) was achieved. Tables of atomic fractional cell coordinates and isotropic thermal parameters (Table A-1), intramolecular bond lengths and angles (Tables A-2 and A-3) are deposited as supplementary material in Appendix A. The structure is similar to that at room temperature. For this reason only the most important features are summarized here.

(i) The asymmetric unit cell contains two *m*-NPIM radicals. Though crystallographically independent, the two molecules (referred to as molecules A and B), especially their imino groups are in ‘nearly equivalent’ positions, closely coinciding upon a $\frac{1}{4}$ translation along the c axis. Fig. 2 shows the structure in projection onto the (ac) crystallographic plane, with the atom labeling scheme used throughout the paper.

(ii) As mentioned above the imino groups of the two molecules have very similar geometry. The N–C–N–O fragment is practically planar.

(iii) The main difference between A and B lies in the orientation and geometry of the nitrophenyl fragments. The interplanar angle between the mean plane of the phenyl cycle and that of the N–O–N–O fragment in A and B is 44.7° and 13.0° respectively. The nitro group plane is rotated to that of the phenyl by 5.7° and 19.2° in molecules A and B.

(iv) The radicals are clearly organized into double chains, stretching along the c crystallographic axis as shown in Fig. 3. The shortest intermolecular contacts in the structure link phenyl carbon atoms of each molecule and the O1 site of the neighbor: C13A and O1B – 3.23 \AA , and C13B and O1A – 3.17 \AA . The contacts are marked in Fig. 2 with dashed lines.

4.2. Spin density reconstruction

The reconstruction of the spatial spin density distribution $S(\mathbf{r})$ from the structure factors $F_M(hkl)$ is a typical Inverse Fourier (IF) problem. Since the data are noisy, the error bars are uneven, the spatial resolution is limited and the sampling of data points in reciprocal space is incomplete and somewhat arbitrary.

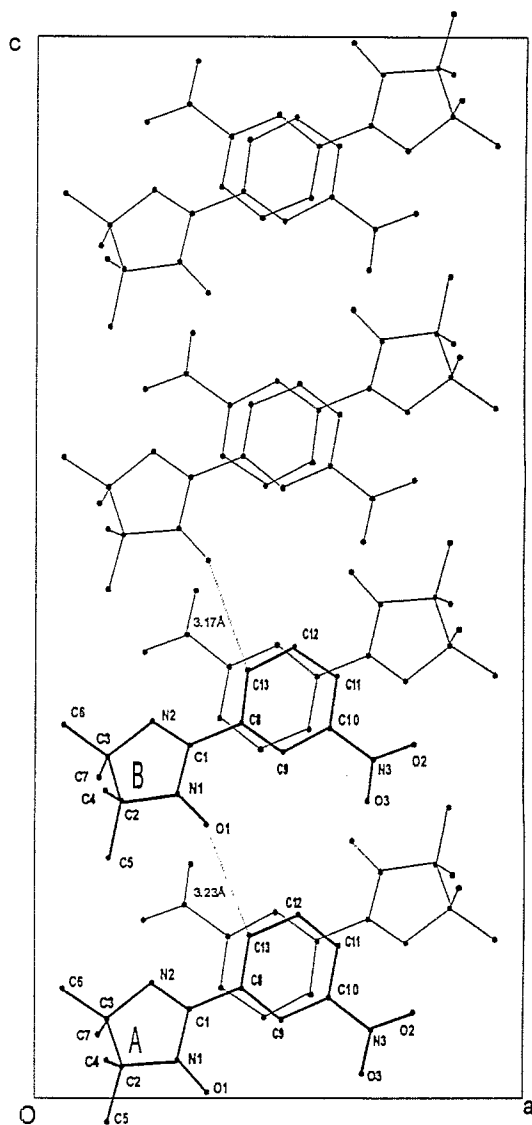


Fig. 2. The crystal structure of $P2_1/c$ m-NPIM in projection onto the (ac) crystallographic plane and the atom labeling scheme. The two molecules in the asymmetric unit cell are shown in bold lines. Close intermolecular contacts dashed.

trary, a straightforward application of the inverse Fourier formula gives rather poor results. This method, known as direct Fourier inversion, ignores the experimental error bars, introduces correlations for which there is no experimental evidence and, since the data are incomplete, makes an arbitrary and unmotivated choice among all the spin density distributions (maps) consistent with the experimental data.

4.2.1. Model-independent spin density

Model-independent methods (Fourier inversion among them) allow to reconstruct the spin density without involving any additional (for example, theoretical) knowledge of what the result should look like. Applying them is very important to test the existing models and to evaluate the quality of the data obtained.

The Maximum of Entropy (MaxEnt) technique [16] selects among all the maps consistent with the experimental data the one with the highest *intrinsic probability*, that is the one which maximizes the configuration entropy of the map [17]. In the 'historic' MaxEnt algorithm which was utilized the criterion of agreement with experiment is chosen simply

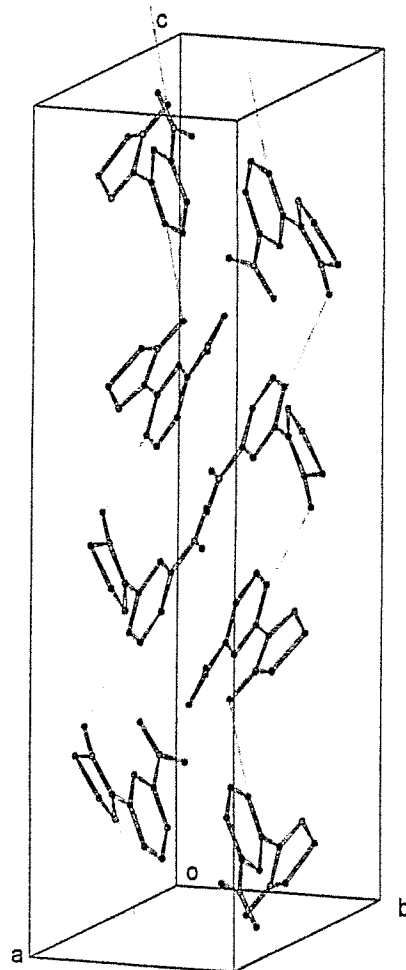


Fig. 3. A view of the crystallographic unit cell.

as $\chi^2 \leq 1$. The method consists in maximizing the entropy functional (1) under this constraint. This procedure is known to give much better results than conventional Fourier inversion and is also model-independent.

$$\text{Entropy}[S(\mathbf{r})] = - \int_{\text{unit cell}} s(\mathbf{r}) \ln s(\mathbf{r}) d^3r, \quad (1a)$$

$$s(\mathbf{r}) = S(\mathbf{r}) / \int_{\text{unit cell}} S(\mathbf{r}) d^3r. \quad (1b)$$

The spin density map was reconstructed in an asymmetric unit cell on a $32 \times 32 \times 32$ array of pixels using a program based on the MEMSYS subroutine package [18]. The thus obtained spin distribution is presented in Fig. 4a in projection onto the O–N–C–N planes of each molecule. Fig. 4b shows the low-level contours. Several important features need to be described here.

(i) The majority of the spin resides on the N1, N2 and O1 atoms, equally shared between those sites.

(ii) On the N1 and O1 sites of both molecules the

density is not centered on the nuclei but is slightly shifted away from the center of the N1–O1 bond. The effect is more pronounced on the N1 site.

(iii) On the central C1 carbon atoms the spin density is *negative*. Moreover, it is off-centered, shifted in the N1–N2 direction.

4.2.2. Magnetic wave function modeling

Another approach to solving the IF problem is to design a parametrized model of the spin density distribution and refine the parameters to best-fit the experimental magnetic structure factors. One representative of this family of reconstruction methods is the magnetic wave function modeling technique which is especially well adapted to treating spin densities in organic free radicals [12]. In this framework an LCAO magnetic wave function $|\psi_i\rangle$ is constructed from standard Slater atomic orbitals at each atomic site i :

$$|\psi_i\rangle = \sum_j \alpha_{i,j} |\phi_j\rangle; \quad (2)$$

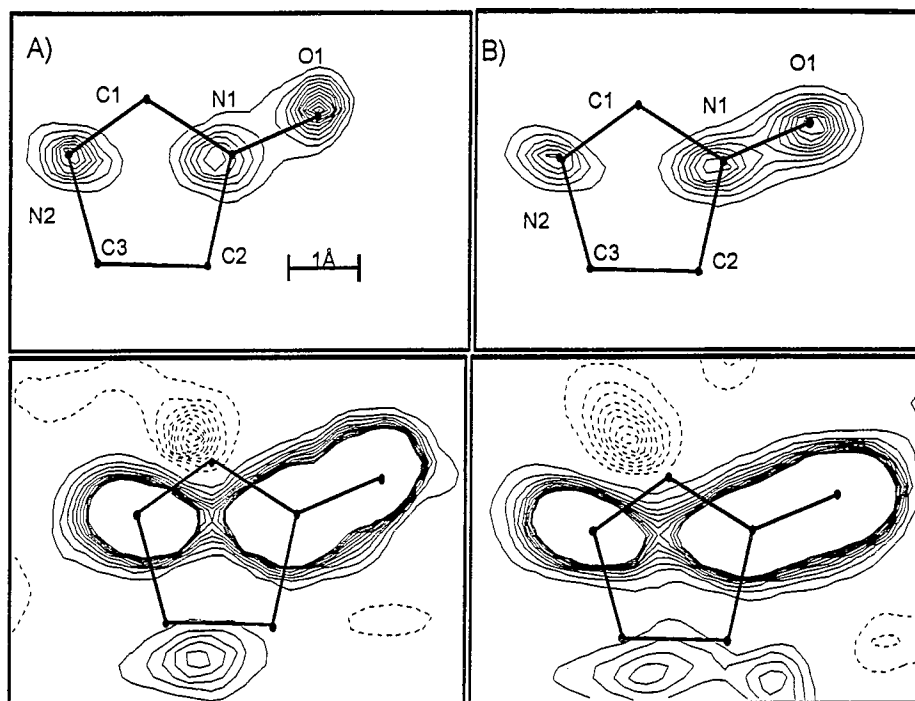


Fig. 4. MaxEnt reconstruction of the spin density in the molecules A and B in projection onto the N–C–N–O planes. $0.05\mu_B/\text{\AA}^2$ (above) and $0.003\mu_B/\text{\AA}^2$ (below) contour steps. Negative contours dashed, zero level contours not shown.

j labels the atomic Slater wave functions ϕ_j and $\alpha_{i,j}$ are the expansion coefficients. The spin density $S(\mathbf{r})$ is expanded as

$$S(\mathbf{r}) = \sum_i S_i \psi_i(\mathbf{r}) \psi_i^*(\mathbf{r}). \quad (3)$$

The coefficients $\alpha_{i,j}$ are scaled to give $\langle \psi_i | \psi_i \rangle = 1$. The individual atomic populations S_i as well as the coefficients $\alpha_{i,j}$ and the radial exponents of the Slater wave functions for each orbital type are the parameters of the model which are refined to best-fit the data. Note that in this model the atomic wave-functions are *first* squared, and *only then* a linear combination is made. In this way we allow for negative spin populations.

For the case of m-NPIM elementary molecular orbital (MO) considerations suggest using $|2p_z\rangle$ orbitals centered on the N1, N2, C1 and O1 atomic sites [19]. The spin density on the other carbon atoms of the imino group is not revealed by MaxEnt and therefore is small and can be reduced to spherical contributions. $|2p'_z\rangle$ and $|2p''_z\rangle$ orbitals make reasonable choices for the phenyl carbon and the NO_2 sites respectively.

The main problem encountered in the particular case of m-NPIM crystals is the nearly equivalent positioning of the molecules A and B. The limitation in spatial resolution and relatively large errors of flipping ratio measurements do not allow to separate the magnetic signal from the two radicals. Therefore, in the model which was actually used, the spin populations of corresponding atoms of A and B were constrained to be equal. In result some sort of an 'average' population is obtained.

The model was refined using a modification of the least-squares program MOLLY [20]. Starting values of the Slater radial exponents were obtained by first principle calculations [21]. They were refined for the N and O atoms only and an agreement $\chi^2 = 2.1$ value obtained. The resulting populations are presented in Table 1. It is obvious that this simple model is inadequate for a correct description of the spin density distribution in the radical, since the resulting value of χ^2 is unacceptably large.

4.2.3. MaxEnt with a reference model

Recently a new method of spin density reconstruction which combines the advantages of tradi-

Table 1

Atomic spin populations (in μ_B) obtained by atomic magnetic wave function modeling and multipolar expansion of spin density

| Site | Wave function modeling | Multipolar expansion |
|------|------------------------|----------------------|
| O1 | 0.322(9) | 0.327(12) |
| N1 | 0.258(9) | 0.269(13) |
| C1 | 0.042(7) | -0.046(8) |
| N2 | 0.193(7) | 0.190(6) |
| C2 | 0.022(8) | 0.022(7) |
| C3 | 0.010(9) | -0.022(9) |
| C4 | 0.005(7) | 0.008(6) |
| C5 | 0.005(10) | 0.005(6) |
| C6 | 0.036(10) | 0.044(9) |
| C7 | 0.001(6) | 0.005(6) |
| C8 | 0.002(6) | 0.002(6) |
| C9 | 0.000(7) | -0.001(7) |
| C10 | 0.007(7) | 0.002(6) |
| C11 | 0.016(7) | -0.013(6) |
| C12 | 0.000(7) | -0.001(6) |
| C13 | 0.002(7) | 0.010(6) |
| N3 | 0.018(5) | -0.013(5) |
| O2 | 0.004(4) | -0.004(4) |
| O3 | 0.018(6) | 0.020(6) |

tional MaxEnt and wave function modeling – MaxEnt reconstruction with an atomic orbital default model (DMME) – was developed [22]. It is based on the extended entropic functional introduced by Skilling [23]. On the one hand, like traditional MaxEnt and unlike model refinement techniques, it allows unlimited freedom of the spin density distribution and always yields a density map which corresponds to $\chi^2 \leq 1$. On the other hand, it allows to incorporate a priori information in the data treatment. This is done in an indirect way. The 'default' model spin density $m(\mathbf{r})$ influences only the entropic functional, that is only the way the 'best' map among those consistent with the data is chosen:

Entropy[$S(\mathbf{r})$]

$$= \int_{\text{unit cell}} S(\mathbf{r}) \left(1 - \ln \left(\frac{S(\mathbf{r})}{m(\mathbf{r})} \right) \right) d^3r. \quad (4)$$

The default model does not in any way restrict the density map itself. If the default model fits the data, the DMME reconstructed density will be identical to the model. If the model is inadequate, the DMME answer will be the one which resembles the model 'as much as possible' and still fits the data. Any

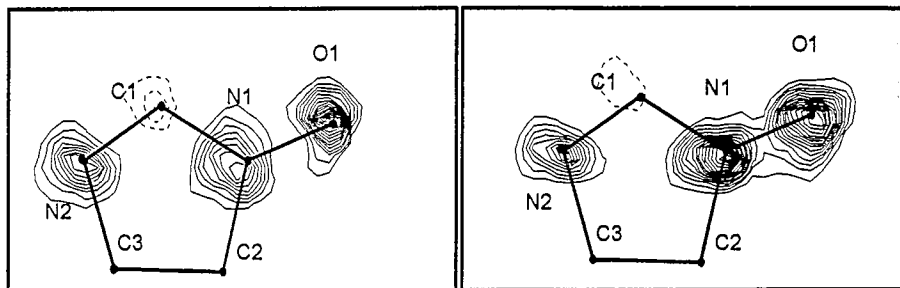


Fig. 5. DMME reconstruction of the spin density in projection onto the N–C–N–O planes of the two molecules. $0.05\mu_B/\text{\AA}^2$ contour step.

deviation of the reconstructed density from the default model is *indeed contained in the experimental data*, since it costs entropy.

The spin density obtained by the refinement method described in the previous section was used as a default model for a DMME reconstruction. The result is shown in Fig. 5. Fig. 6 visualizes the difference between the DMME answer and the default model. It is clearly seen why the default model fails to fit the experimental data.

(i) The large positive spin density on the O1 and N1 sites is *not centered* on these atoms, but shifted outwards, away from the O1–N1 bond center.

(ii) The spin density on N2 is slightly asymmetrical, being ‘pushed away’ from C1.

(iii) On both molecules the negative density on C1 is off-centered, being shifted in the N1–N2 direction.

This deformation of the spin density, observed on both radicals, may not be accounted for by the *axially symmetrical* atomic p orbitals used in the default model. A more advanced model should allow

more freedom for the *shape* of the spin density distribution.

4.2.4. Multipolar expansion of the spin density

The flexibility of the simple atomic orbital model was increased by direct modeling the spin density, instead of modeling the magnetic wave function. In the vicinity of the nuclei the spin density was expanded into a multipolar series [12]:

$$S(\mathbf{r}) = \sum_l R^l(r) \sum_{m=-l}^l \alpha_l^m y_l^m(\hat{\mathbf{r}}); \quad (5)$$

y_l^m are real spherical harmonics, R^l are standard Slater radial functions and α_l^m are the population coefficients. Though more flexible, this model uses far too many variables to describe a single atom. This hinders the convergence of the least-squares algorithm and, since the correlations between the parameters are large (nuisance parameters), their values become ill-defined. Depending on the quality and quantity of the experimental data available, an

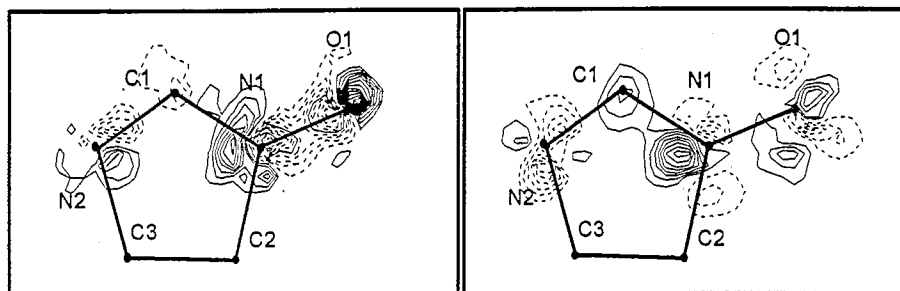


Fig. 6. Difference between the DMME reconstruction and the default model in projection onto the N–C–N–O planes of the two molecules. $0.02\mu_B/\text{\AA}^2$ contour step.

Table 2

Multipolar expansion of the spin density: refinement statistics and refined parameters not included in Table 1

| Refinement statistics | |
|--|------------|
| N_{vars} | 29 |
| N_{obs} | 248 |
| χ^2 | 1.6 |
| weighted r-factor | 0.17 |
| Refined multipolar expansion coefficients | |
| O1 monopole (spin population) | 0.327(13) |
| O1 dipole y | -0.017(10) |
| O1 quarupole z^2 | 0.172(25) |
| O1 octupole yz^2 | -0.013(82) |
| O1 octupole y^3 | -0.050(42) |
| N1 monopole (spin population) | 0.269(13) |
| N1 dipole y | 0.024(9) |
| N1 quarupole z^2 | 0.091(25) |
| N1 octupole yz^2 | 0.119(77) |
| N1 octupole y^3 | -0.010(44) |
| Refined Slater exponents, inverse Bohr radii | |
| ζ_0 | 4.74(24) |
| ζ_N | 4.73(25) |

optimal basis of spherical harmonics should be chosen for each nuclear site. For the case of m-NPIM the following model was used:

(i) As before, the spin distributions in the two molecules were constraint to be equal.

(ii) The expansion (5) was used only for the N1 and O1 sites, where a *strong* deformation of a *large* spin density was observed. For all the other sites the atomic orbital description of the spin density was kept.

(iii) For N1 and O1 only those spherical harmonics which are even with respect to \hat{z} and \hat{x} (axis \hat{x} is chosen perpendicular to \hat{z} and to the O1–N1 bond, the \hat{y} axis) and which correspond to $l \leq 3$ were included into the expansion.

The refined values of atomic spin populations are listed in Table 1, the other refined parameters and the refinement statistics are presented in Table 2. Fig. 7 shows the obtained spin density in projection onto the N–C–N–O molecular plane and Fig. 8 – onto the (zy) plane. Notably, this model only gives a crude description of the spin density shape. Nevertheless, the achieved agreement with experiment $\chi^2 = 1.6$ shows that it describes the spin density in the

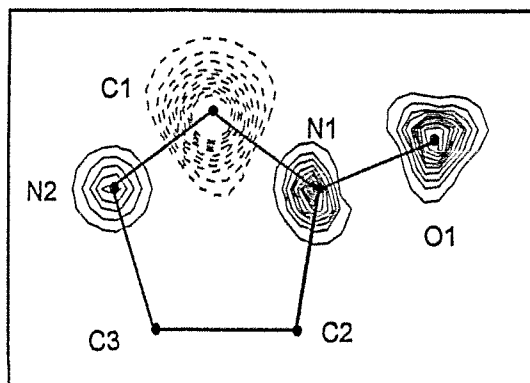


Fig. 7. Multipolar expansion reconstruction of the spin density in projection onto the N–C–N–O plane. $0.1 \mu_B / \text{\AA}^2$ contour step for positive density. Negative contours ($0.008 \mu_B / \text{\AA}^2$ step) dashed.

compound much better than the one based on axially symmetrical p-orbitals.

4.3. *Ab initio* calculations

First principle calculations of the spin density distribution in m-NPIM were also carried out. These were performed for the two m-NPIM molecules using the experimental molecular geometry. We have applied the density functional theory (DFT) as implemented in the program DMol [24]. At the local spin density functional level the functional of Vosko, Wilk and Nusair (VWN) [25] was used. The DMol program uses atomic-like basis sets [26] which recover the DFT dissociation limit exactly.

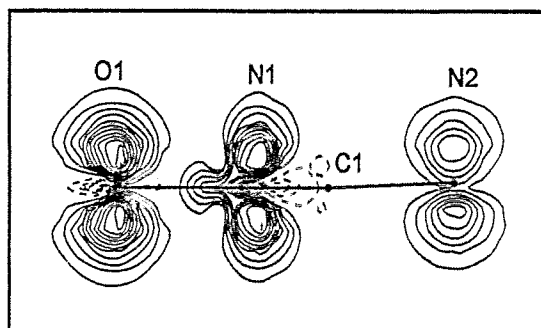


Fig. 8. Multipolar expansion reconstruction of the spin density in projection onto the plane which contains the N–O bond and is perpendicular to the C1–N1–O1 plane. $0.05 \mu_B / \text{\AA}^2$ contour step. Negative contours dashed.

Table 3

Experimental (scaled to $1\mu_B$ per radical) and theoretical spin populations of Im3NO atoms. The theoretical values (Mulliken populations) are obtained by density functional first principle calculations

| Site | Experiment | DFT | |
|------|------------|------------|------------|
| | | Molecule A | Molecule B |
| O1 | 0.407(15) | 0.457 | 0.429 |
| N1 | 0.335(16) | 0.293 | 0.287 |
| C1 | -0.057(10) | -0.032 | -0.033 |
| N2 | 0.236(7) | 0.274 | 0.284 |
| C2 | 0.027(9) | -0.007 | -0.007 |
| C3 | -0.027(11) | -0.003 | -0.006 |
| C4 | 0.010(7) | 0.031 | 0.026 |
| C5 | 0.006(7) | 0.008 | 0.010 |
| C6 | 0.055(11) | 0.004 | 0.005 |
| C7 | 0.006(7) | 0.015 | 0.018 |
| C8 | 0.002(7) | 0.002 | 0.003 |
| C9 | -0.001(9) | -0.003 | -0.006 |
| C10 | 0.002(7) | 0.000 | 0.001 |
| C11 | -0.016(7) | -0.002 | -0.003 |
| C12 | -0.001(7) | 0.000 | 0.001 |
| C13 | 0.012(7) | -0.002 | -0.002 |
| N3 | -0.016(6) | 0.000 | 0.000 |
| O2 | -0.005(5) | 0.000 | 0.000 |
| O3 | 0.026(7) | 0.000 | 0.000 |

The individual atomic Mulliken spin populations for the two m-NPIM molecules are tabulated in Table 3 together with experimental values. The latter are scaled to $1\mu_B/f.u.$ The projection of the spin density, calculated for molecule A is given in Fig. 9 in projection onto the N–C–N–O plane.

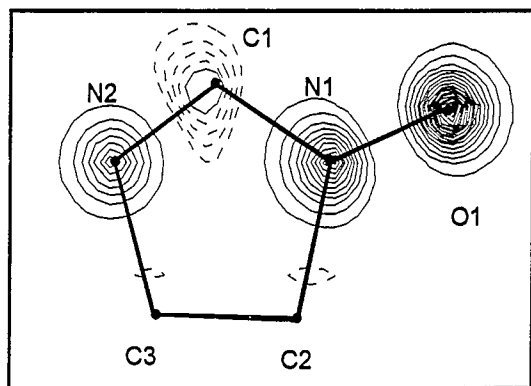


Fig. 9. Density functional theoretical spin density in projection onto the N–C–N–O planes of the two molecules. $0.02\mu_B/\text{\AA}^2$ contour step for positive density. Negative contours (0.002 step) dashed.

5. Discussion

As already mentioned, in the studied $P2_1/c$ form of m-NPIM there are two crystallographically independent radicals. Since these have similar geometry, the equivalence of the two spin density distributions imposed by the multipolar modeling should not lead to significant errors. It is confirmed by the fact that a reasonable agreement with experiment was achieved in the refinement and by the similarity of ab initio spin densities obtained for the two geometries. Also, MaxEnt methods do *not* treat the two molecules as equivalent, and yet yield for them similar spin distributions.

5.1. The imino group

(i) As may be seen from MaxEnt reconstructions, most of the spin density is concentrated on the imino group and is located on the N1, N2 and O1 atoms. Here the major contribution arises from the spin delocalization (SD) effect and may be attributed to the unpaired electron residing on the singly occupied molecular π orbital (SOMO).

Model refinement methods provide additional quantitative information. On the whole, the spin density is increasing towards the O1 oxygen site, the atomic spin population of the latter being the largest and the spin residing on the neighboring N1 greater, than that on N2. The O1 : N1 : N2 spin partitioning is approximately 41 : 34 : 24.

(ii) The spin density on N1 and O1 is *not centered* on the nuclei. Instead, it is shifted outwards, towards the periphery, away from the N–O bond center. As may be seen in Fig. 8, the spin carrying atomic p-orbitals become ‘bent’. The shifting is what one would expect from the antibonding nature of the SOMO (from the subtraction of two p_z atomic orbitals (AO’s) when constructing an LCAO SOMO). This indicates, that the SOMO has a node on the N1–O1 bond. The multipolar expansion of spin density performed in this work allows to account for the deformation of spin density only crudely. Nevertheless, the model provides a reasonable approximation.

It is not the first time that this sort of spin density deformation was observed in organic radicals. It was already encountered in our polarized neutron diffraction studies of the tetracyanoethylene radical-ion

[27,28]. Ab initio DFT calculations for m-NPIM also predicts this effect as may be seen from Fig. 9, though the experimental deformation of the spin density is more pronounced.

(iii) The bridging sp^2 carbon atom C1, unlike the bridging carbon in nitronyl nitroxides [5], is not necessarily a node of the SOMO and a priori there is no reason for its spin population to be small or negative. Experimentally a negative C1 spin population is observed. The effect is less pronounced than in nitronyl nitroxides. In the latter, it is exclusively due to the spin polarization (SP) effect [29]. On the contrary, in m-NPIM it is the result of competition between SP and SD. The contribution of C1 AOs to the SOMO is rather small and the SD and SP spin densities on C1 are of the same order of magnitude, the latter being slightly larger, providing a negative total population.

(iv) MaxEnt, as well as DFT calculations, show an asymmetrical deformation (off-centering, shifting in the N1–N2 direction) of the negative spin on C1. This is accompanied by a slight shifting of the positive spin density on N1 towards the C1 atom on the one hand, and, on the other hand, a shifting of the positive spin density on N2 away from C1.

A simple illustrative explanation may be given by considering the structure of the SOMO. This orbital of m-NPIM has two nodes. As follows from the discussion above, one node is definitely located in between the N1 and O1 sites. The other node is on the N1–C1 or else the C1–N2 bond. The SOMO is thus bonding on either N2–C1 or C1–N1. Consequently, the positive spin density on N1 and N2 becomes deformed, shifted towards or away the C1 site. It is the second case which is realized in m-NPIM. The SOMO is thus bonding on C1–N1 and antibonding on C1–N2 and N1–O1.

The positive contribution to the spin density on C1 becomes shifted too, along the N2–N1 direction. The SP effect, which is liable for the *negative* (dominating) contribution to the C1 total spin, involves the polarization of the frontier orbitals of the radical. These are otherwise antibonding on *both* C1–N1 and C1–N2 (the lowest unoccupied MO), or bonding on C1–N2 and antibonding on C1–N1 (the highest occupied MO). In consequence, the *negative* spin density on C1 is *not* shifted at all, or shifted in the N1–N2 direction opposite to the shifting of the

positive spin density. In consequence the *total* spin density becomes deformed.

5.2. The nitrophenyl group

The spin populations of the nitrophenyl group atoms are at the limit of experimental accuracy. Nevertheless, at the qualitative level, the spin transfer to the aromatic and nitro fragments is similar to that observed previously in related radicals [5,6]. For example, in the phenyl substituted nitronyl nitroxide weak alternating $\cdots + / - / + / - \cdots$ populations of the phenyl ring carbon atoms were found [5]. More or less, this sign alternation is present in the m-NPIM radical as well.

5.3. Comparison with ab initio calculations

The results obtained by density functional calculations are quite satisfactory. Even though the unbalance of N1/N2 spin populations is not predicted, the spin population of the O1 site is found to be greater than those of nitrogen sites, in agreement with experiment. Such important features as the deformation of the spin density on the N1–O1 bond, the small negative spin on C1 and its off-centering are also recovered by the first principle approach. The spin polarization of the nitrophenyl group is underestimated. In contrast to what was observed experimentally, no spin density transfer to the NO_2 group is found. This obviously results from the vanishing of calculated spin density on the C10 phenyl carbon site. Also, the influence of the neighboring radicals in the crystal as demonstrated in our previous works [5,6,27,30,31], contrary to Hartree–Fock based methods, density functional calculations do not exaggerate the spin polarization effect. It seems that they do however underestimate it instead.

6. Conclusion

The polarized neutron diffraction determination of the spin distribution in the $P2_1/c$ form of the meta-nitrophenyl imino nitroxide free radical has been performed. The high quality data obtained in this experiment and the sophisticated data treatment tech-

niques allowed to obtain precise quantitative results in terms of atomic spin populations. In addition, important qualitative information pertaining to the *shape* of the spin density distribution was obtained.

Our data provide new insight on the spin polarization phenomena and the *orbital structure* of the radical. The study of the spin density transfer to the nitrophenyl group allows to give a qualitative expla-

nation of the intermolecular antiferromagnetic interaction.

The recently developed DMME technique proves to be a powerful and flexible method for polarized neutron diffraction data treatment.

Finally, the density functional first principle calculations give quite acceptable results, but slightly underestimate the spin polarization effect.

Appendix

Table A-1

Atomic fractional cell coordinates and isotropic thermal parameters of $P2_1/c$ m-NPIM crystals at temperature 30 K by single-crystal neutron diffraction; $a = 13.15(3)$ Å, $b = 7.29(2)$ Å, $c = 26.98(4)$ Å and $\beta = 97.45(11)^\circ$

| Site | Molecule A | | | | Molecule B | | | |
|------|-----------------|-----------------|-----------------|----------|-----------------|-----------------|-----------------|----------|
| | $X \times 10^4$ | $Y \times 10^4$ | $Z \times 10^4$ | b_{eq} | $X \times 10^4$ | $Y \times 10^4$ | $Z \times 10^4$ | b_{eq} |
| O1 | 3535(3) | 5942(8) | 56(1) | 0.42(9) | 3511(3) | 5133(9) | 2577(1) | 0.76(9) |
| O2 | 7754(3) | 7789(8) | 808(2) | 0.94(10) | 7765(3) | 7009(9) | 3328(2) | 1.19(11) |
| O3 | 6714(3) | 8735(8) | 230(1) | 0.78(10) | 6806(3) | 5500(8) | 2798(1) | 0.75(9) |
| N1 | 2927(2) | 6718(5) | 356(1) | 0.46(6) | 2924(2) | 5959(5) | 2866(1) | 0.49(6) |
| N2 | 2407(2) | 7890(5) | 1081(1) | 0.79(7) | 2401(2) | 7457(5) | 3544(1) | 0.50(7) |
| N3 | 6889(2) | 8044(5) | 640(1) | 0.75(9) | 6938(2) | 6378(5) | 3181(1) | 0.83(6) |
| C1 | 3171(3) | 7333(7) | 836(1) | 0.37(9) | 3176(3) | 6769(7) | 3322(1) | 0.53(9) |
| C2 | 1798(3) | 6636(8) | 290(1) | 0.72(9) | 1794(2) | 5046(7) | 2796(1) | 0.28(8) |
| C3 | 1487(3) | 7849(7) | 742(1) | 0.37(9) | 1493(3) | 7332(8) | 3212(1) | 0.76(10) |
| C4 | 1480(3) | 4589(8) | 352(1) | 0.85(9) | 576(3) | 6765(8) | 3512(1) | 0.61(9) |
| H1 | 684(6) | 4454(16) | 296(3) | 2.93(19) | -93(6) | 6597(15) | 3286(3) | 2.28(19) |
| H2 | 1699(5) | 4083(15) | 713(3) | 2.17(18) | 358(6) | 7881(15) | 3786(3) | 2.76(21) |
| H3 | 1873(6) | 3770(16) | 71(3) | 3.30(21) | 728(6) | 5489(17) | 3729(3) | 2.09(19) |
| C5 | 1490(3) | 7330(7) | -222(1) | 0.63(9) | 1310(3) | 9306(8) | 3018(1) | 0.78(8) |
| H4 | 664(6) | 7408(15) | -263(3) | 2.73(21) | 613(5) | 9368(16) | 2788(2) | 2.31(19) |
| H5 | 1775(6) | 6358(16) | -513(3) | 3.33(21) | 1934(6) | 9796(16) | 2806(2) | 2.42(18) |
| H6 | 1809(6) | 8704(16) | -308(3) | 2.71(19) | 1227(6) | 241(16) | 3330(3) | 2.76(19) |
| C6 | 571(3) | 7161(8) | 1025(1) | 0.72(10) | 1443(3) | 3982(7) | 2893(1) | 0.43(8) |
| H7 | -104(6) | 7082(15) | 782(3) | 2.28(19) | 625(6) | 3833(15) | 2835(3) | 2.55(19) |
| H8 | 463(6) | 8108(14) | 1332(3) | 1.77(18) | 1654(5) | 3531(14) | 3283(3) | 1.85(18) |
| H9 | 703(5) | 5786(16) | 1175(3) | 2.19(18) | 1801(6) | 3020(15) | 2633(3) | 2.41(20) |
| C7 | 1305(3) | 9874(7) | 592(1) | 0.35(8) | 1512(3) | 6496(8) | 2262(1) | 0.42(9) |
| H10 | 596(6) | 55(16) | 368(2) | 2.60(18) | 686(6) | 6632(14) | 2222(2) | 2.03(18) |
| H11 | 1936(5) | 423(15) | 386(2) | 1.75(17) | 1765(5) | 5442(15) | 2017(3) | 2.17(17) |
| H12 | 1219(6) | 712(16) | 919(3) | 2.90(19) | 1814(6) | 7764(15) | 2157(3) | 1.85(19) |
| C8 | 4237(3) | 7236(7) | 1037(1) | 0.46(9) | 4220(3) | 6889(7) | 3531(1) | 0.51(9) |
| C9 | 5052(3) | 7700(7) | 734(1) | 0.65(9) | 5078(3) | 6459(7) | 3253(1) | 0.48(9) |
| H13 | 4935(6) | 8156(14) | 366(3) | 2.21(19) | 5017(5) | 6063(13) | 2876(3) | 1.50(17) |
| C10 | 6024(3) | 7531(7) | 945(1) | 0.30(9) | 6040(3) | 6739(7) | 3480(1) | 0.78(9) |
| C11 | 6218(3) | 6922(7) | 1430(1) | 0.79(9) | 6178(3) | 7317(7) | 3965(1) | 0.43(9) |
| H14 | 6992(6) | 6772(15) | 1568(2) | 1.79(19) | 5402(6) | 8159(14) | 4618(3) | 2.15(19) |
| C12 | 5389(3) | 6515(7) | 1721(1) | 0.64(9) | 5305(3) | 7673(7) | 4242(1) | 0.42(9) |
| H15 | 5523(5) | 6070(13) | 2102(2) | 1.53(17) | 6942(6) | 7508(13) | 4121(3) | 1.58(19) |
| C13 | 4395(3) | 6664(7) | 1528(1) | 0.34(9) | 4343(3) | 7491(7) | 4025(1) | 0.65(10) |
| H16 | 3749(6) | 6537(15) | 1760(3) | 1.99(18) | 3677(6) | 7788(14) | 4230(3) | 1.79(18) |

Table A-2
Intramolecular bond lengths for molecules A and B

| Bond | Distance (Å) | |
|---------|--------------|----------|
| | A | B |
| O1–N1 | 1.257(1) | 1.240(1) |
| O2–N3 | 1.248(2) | 1.255(2) |
| O3–N3 | 1.241(1) | 1.231(1) |
| N1–C1 | 1.415(1) | 1.410(1) |
| N1–C2 | 1.501(3) | 1.504(3) |
| N2–C1 | 1.256(2) | 1.272(2) |
| N2–C3 | 1.536(2) | 1.513(2) |
| N3–C10 | 1.438(2) | 1.438(2) |
| C1–C8 | 1.517(3) | 1.501(3) |
| C2–C3 | 1.554(1) | 1.553(1) |
| C2–C4 | 1.558(3) | 1.549(1) |
| C2–C5 | 1.535(1) | 1.525(3) |
| C3–C6 | 1.496(2) | 1.495(2) |
| C3–C7 | 1.551(3) | 1.552(3) |
| C8–C9 | 1.372(2) | 1.376(2) |
| C9–C10 | 1.418(2) | 1.434(2) |
| C10–C11 | 1.410(1) | 1.391(1) |
| C11–C12 | 1.360(2) | 1.380(2) |
| C12–C13 | 1.424(3) | 1.413(2) |
| C13–C8 | 1.411(1) | 1.416(1) |

Table A-3
Intramolecular bond angles for molecules A and B

| Bond | Angle (°) | |
|-------------|-----------|-------|
| | A | B |
| O1–N1–C1 | 125.2 | 126.7 |
| O1–N1–C2 | 121.4 | 121.3 |
| C1–N1–C2 | 111.7 | 111.5 |
| C1–N2–C3 | 108.2 | 109.3 |
| O2–N3–O3 | 125.2 | 126.6 |
| O2–N3–C10 | 117.9 | 117.5 |
| O3–N3–C10 | 117.0 | 115.8 |
| N1–C1–N2 | 112.8 | 111.9 |
| N1–C1–C8 | 123.0 | 126.1 |
| N2–C1–C8 | 124.1 | 121.9 |
| N1–C2–C3 | 97.2 | 98.0 |
| N1–C2–C4 | 106.8 | 106.3 |
| N1–C2–C5 | 112.2 | 112.0 |
| C3–C2–C4 | 113.3 | 114.6 |
| C3–C2–C5 | 116.7 | 116.1 |
| C4–C2–C5 | 109.6 | 108.9 |
| N2–C3–C2 | 106.4 | 106.1 |
| N2–C3–C6 | 109.8 | 109.5 |
| N2–C3–C7 | 105.4 | 106.0 |
| C2–C3–C6 | 113.8 | 113.5 |
| C2–C3–C7 | 112.1 | 113.5 |
| C6–C3–C7 | 109.0 | 108.0 |
| C1–C8–C9 | 119.4 | 121.8 |
| C1–C8–C13 | 120.5 | 120.1 |
| C9–C8–C13 | 120.0 | 118.2 |
| C8–C9–C10 | 116.0 | 117.1 |
| N3–C10–C9 | 117.1 | 117.1 |
| N3–C10–C11 | 117.1 | 117.3 |
| C9–C10–C11 | 125.8 | 125.6 |
| C10–C11–C12 | 116.4 | 116.1 |
| C11–C12–C13 | 120.2 | 120.0 |
| C8–C13–C12 | 121.6 | 123.0 |

References

- [1] Recent reviews on molecular magnetism: (a) A. Caneschi, D. Gatteschi and P. Rey, *Prog. Inorg. Chem.* 39 (1991) 331; (b) O. Kahn, *Molecular Magnetism* (VCH Publishers, 1993); (c) J.S. Miller and A.J. Epstein, *Angew. Chem. Int. Ed. Engl.* 33 (1994) 385.
- [2] (a) J.X. Boucherle, B. Gillon, E. Ressouche, P. Rey and J. Schweizer, *Physica B* 180 & 181 (1992) 142; (b) J.X. Boucherle, B. Gillon, E. Ressouche, P. Rey and J. Schweizer, *Z. Naturforsch.* a48 (1993) 120; (c) E. Ressouche, J.X. Boucherle, B. Gillon, P. Rey and J. Schweizer, *J. Am. Chem. Soc.* 115 (1993) 3610.
- [3] (a) M. Tamura, Y. Nakazawa, D. Shiomi, K. Nozawa, Y. Hosokoshi, M. Ishikawa, M. Takahashi and M. Kinoshita, *Chem. Phys. Lett.* 186 (1991) 401; (b) Y. Nakazawa, M. Tamura, N. Shirakawa, D. Shiomi, M. Takahashi, M. Kinoshita and M. Ishikawa, *Phys. Rev. B* 46 (1992) 8906; (c) M. Kinoshita, *Mol. Cryst. Liq. Cryst.* 232 (1993) 1.
- [4] (a) A. Rassat, R. Chiarelli and P. Rey, *J. Chem. Soc. Chem. Commun.* (1992) 1081; (b) R. Chiarelli, M.A. Novak, A. Rassat and J.L. Tholence, *Nature* 363 (1993) 147; (c) R. Chiarelli, A. Rassat, Y. Dromzee, Y. Jeannin, M.A. Novak and J.L. Tholence, *Physica Scripta* T49 (1993) 706.
- [5] (a) E. Ressouche, A. Zheludev, J.X. Boucherle, B. Gillon, P. Rey and Schweizer, *J. Mol. Cryst. Liq. Cryst.* 232 (1993) 13; (b) A. Zheludev, V. Barone, M. Bonnet, B. Delley, A. Grand, E. Ressouche, P. Rey, R. Subra and J. Schweizer, *J. Am. Chem. Soc.* 116 (1994) 2019.
- [6] A. Zheludev, M. Bonnet, E. Ressouche, J. Schweizer, M. Wan and H. Wang, *J. Magn. Magn. Mater.* 135 (1994) 147.
- [7] E.F. Ullman, L. Call and J.H. Osiecki, *J. Org. Chem.* 11 (1970) 3623.
- [8] F. Lanfranc de Panthou, D. Luneau, J. Laugier and P. Rey, *J. Am. Chem. Soc.* 115 (1993) 9095.
- [9] D. Luneau, P. Rey, J. Laugier, P. Fries, A. Caneschi, D. Gatteschi and R. Sessoli, *J. Am. Chem. Soc.* 113 (1991) 1245.
- [10] D. Luneau, P. Rey, E. Belorizky and A. Cogne, *Inorg. Chem.* 31 (1992) 3578.
- [11] P. Rey and D. Luneau, Review on imino nitroxides, in preparation.
- [12] B. Gillon and J. Schweizer, Study of Chemical Bonding in Molecules: The interest of Polarized Neutron Diffraction, in: *Molecules in Physics, Chemistry and Biology*, Vol. 2, ed. Jean Maruani (Kluwer Academic, 1989) pp. 111–147.
- [13] Unpublished X-ray data by D. Luneau.

- [14] M.S. Lehmann and F.K. Larsen, *Acta Cryst. B* 26 (1970) 1198.
- [15] W.R. Busing, K.O. Martin and H.A. Levy, *Rapport ORNL 59-4-37*, Oak Ridge National Laboratory, Oak Ridge, Tennessee (1991).
- [16] (a) R.J. Papoular and B. Gillon, in: *Neutron Scattering Data Analysis Inst. Phys. Conf. Ser. 107*, ed. M.W. Johnson Bristol (1990) p. 101; *Europhys. Lett.* 13 (1992); (b) R.J. Papoular and J. Schweizer, *Procs. 6th Int. Neutron School on Neutron Physics, Alushta, USSR 8–18 October 1991* p. 170; (c) R.J. Papoular, E. Ressouche, J. Schweizer and A. Zheludev, in: *Fundamental Theories in Physics, Vol. 53, Maximum Entropy And Bayesian Methods*, eds. A. Mohammad-Djafari and G. Demoment (Kluwer Academic, 1993) p. 311.
- [17] (a) S.F. Gull and G.J. Daniell, *Nature* 272 (1978) 686; (b) J. Skilling and S.F. Gull, in: *Maximum Entropy and Bayesian Methods in Inverse Problems*, eds. C. Ray Smith and W.T. Grandy, Jr. (Reidel, Dordrecht, 1985).
- [18] S.F. Gull and J. Skilling, *MEMSYS Users' Manual*, Maximum Entropy Data Consultants Ltd, 33 North End, Meldreth, Royston SG8 6NR, England (1989).
- [19] We define the following axes: z is normal to the N–C–N–O mean plane, z' to the mean plane of the phenyl ring, and z'' to the O2–N3–O3 plane.
- [20] N.K. Hansen and P. Coppens, *Acta Cryst. A* 34 (1978) 909.
- [21] N.J. Hehre, R.F. Stewart and J.A. Pople, *J. Chem. Phys.* 51 (1969) 2657.
- [22] A. Zheludev, R.J. Papoular, E. Ressouche and J. Schweizer, A reference model for Maximum of Entropy density reconstructions from diffraction data, in preparation for *Acta Cryst. A*.
- [23] J. Skilling, *The Axioms of Maximum Entropy*, in: *Maximum Entropy and Bayesian Methods in Science and Engineering*, Vol. 1, eds. G.J. Erickson, C.R. Smith (Kluwer Academic, 1988) pp. 173–187.
- [24] DMol, Biosym Technologies Inc., 9686 Scranton road, San Diego, CA 92121–2777, USA.
- [25] S.H. Vosko, L. Wilk and M. Nausair, *Can. J. Phys.* 58 (1980) 1200.
- [26] B. Delley, *J. Chem. Phys.* 92 (1990) 508; B. Delley, *J. Chem. Phys.* 94 (1991) 7245.
- [27] A. Zheludev, A. Grand, E. Ressouche, J. Schweizer, B. Morin, A.J. Epstein, D. Dixon and J.S. Miller, *Angew. Chem.* 33 (1994) 1397.
- [28] A. Zheludev, A. Grand, E. Ressouche, J. Schweizer, B. Morin, A.J. Epstein, D. Dixon and J.S. Miller, *J. Am. Chem. Soc.* 116 (1994) 7243.
- [29] I. Nakajitsuji, *J. Chem. Phys.* 59 (1973) 2586.
- [30] D. Bordeau, J.X. Boucherle, B. Delley, B. Gillon, E. Ressouche and J. Schweizer, *Z. Naturforsch.* a48 (1993) 117.
- [31] B. Delley, P. Becker and B. Gillon, *J. Chem. Phys.* 80 (1984) 4286.